Speeding-up Defect Analysis and Modeling of Graphene based Tunnel Field Effect Transistors

A THESIS
SUBMITTED TO THE FACULTY OF
UNIVERSITY OF MINNESOTA
BY

AKHILESH RAMLAUT JAISWAL

IN PARTIAL FULFILLMENT OF THE REQUIREMENTS
FOR THE DEGREE OF
MASTER OF SCIENCE

Kiarash Bazargan, Adviser

May, 2014

Acknowledgements

I would like to thank my advisor Prof. Kiarash Bazargan for his guidance and advice. I appreciate his patience in mentoring and guiding me throughout the work. I have learned how to approach problem solving and avoid digressions while conducting research. I would like to thank Prof. Ted Higman for helpful discussions. My special thanks to Ed Pataky for introducing me to simulation tools used in this work. Last but not the least, I express my gratitude to my parents for their constant support and encouragement.

Abstract

The hunt for post-CMOS devices has seen emergence of many new devices and materials, one among those is graphene based Tunnel Field Effect Transistor (TFET). It becomes necessary to investigate device-circuit and device-system co-design to tackle some of the challenges posed by these devices. Defect analysis and related data is necessary to study variation and effects that realistic devices would have on system level. Such defect analyses require quantum mechanical analyses and are compute and time intensive. In order to quickly gain insight and hence speed up defect analysis for graphene based TFET devices, we have developed a bandstructure based filtering mechanism which filters out severely defected devices from a pool of devices under study thus saving computation time. Effort has also been made to develop a compact model based on Landauer equation for ballistic transport and analytical expression for quantum mechanical tunneling.

Table of Contents

List of Figures

1. Introduction

1.1. Limits of MOSFET

The scalability of Metal Oxide Semiconductor Field Effect Transistor (MOSFET) has been major factor driving Moore's Law for over 40 decades. However, scaling brings with it higher standby power dissipation due to the so called short channel effects. Such leakage mechanism and ways to counter them has been widely studied by K. Roy et al. and others [1]. Despite extensive research there remains a fundamental limit to the extent one can reduce leakage power. This is governed by a feature called sub-threshold slope. Sub-threshold slope is a measure of reduction in *OFF* current of MOSFET with respect to controlling voltage and has fundamental limit of 60mV/decade at temperature of 300K.

This theoretical limit is governed by the very principle on which MOSFETs work as shown by M. Lundstrom et al. [2]. Fig. 1 shows the conduction band edge versus position for a MOSFET under different bias conditions. Electrons in thermal equilibrium reservoir, the Source (S) face a potential barrier of height qV_{bi} Joules where q is electronic charge, V_{bi} is in Volts (fig. 1). When a positive voltage V_{GS} is applied between the Gate (G) and source terminal, the barrier height reduces, electrons can now cross the barrier and get into the *channel* region; these electrons can be collected by the Drain (D) with a positive voltage of V_{DS} between drain and source (fig. 1 solid lower curve). This flow of electrons constitute drain current (I_{D_ON}) and the device is said to be *ON*. In absence on V_{GS}, only very few electrons can get into channel region and constitute current (I_{D_OFF}) (fig.1), the device is said to be in *OFF* state or sub-threshold

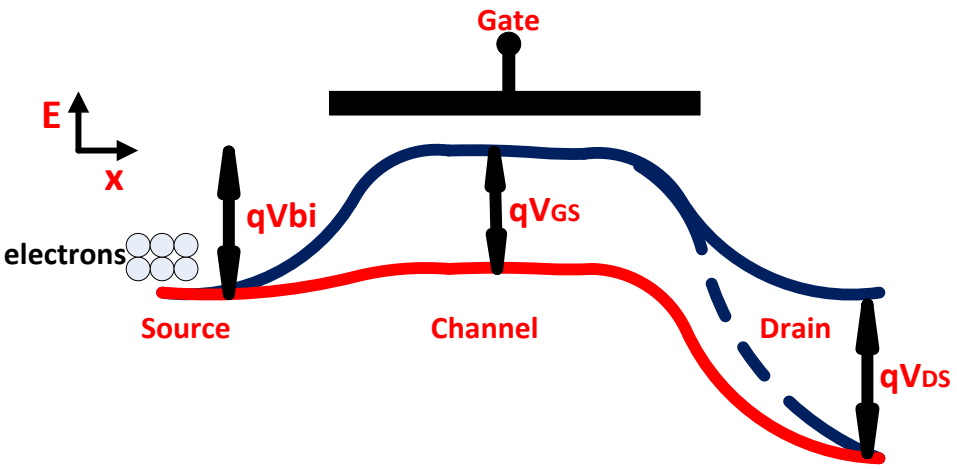

Figure 1. Conduction band edge versus position, for a MOSFET. Solid upper line is for V_{GS} = 0 and V_{DS} =0; solid lower line is for finite V_{GS} and V_{DS} (*ON* state), dashed line is for V_{GS} = 0 and finite V_{DS} (*OFF* state).

region.

The mechanism by which electrons cross the barrier and enter the channel region in sub-threshold operation is Thermionic Emission. For a barrier of height ø, the total electron current (*J*) over the barrier is given by [3]

$$J = AT^2 exp\left(\frac{-q\emptyset}{kT}\right) \quad (1)$$

Where *A* is Richardson constant, *T* is temperature, *k* is Boltzmann's constant. It is this exponential dependence on barrier height ø, which results in a sub-threshold slope (SS), defined as inverse slope of *log(Id)* versus V_{GS} characteristic in sub-threshold region of operation, given by

$$SS = ln10\frac{kT}{q}\left(1 + \frac{Cd}{Cox}\right) \quad (2)$$

Where C_d is depletion capacitance in channel region and C_{ox} is oxide capacitance. If C_{ox} tends to ∞, SS = 60mV/decade at 300K.

Lower SS would mean steeper cutoff characteristic and hence lower leakage current. Based on equation (1), the only way to go below 60mV/decade is by reducing temperature, which is not a viable option. Any switch, whose sub-threshold characteristic does not depend on the exponential thermionic emission phenomenon, could possibly result in lower SS and hence lower power.

Tunnel Field Effect Transistors (TFETs) reviewed by A. Seabaugh et al. [4] that carry current due to quantum mechanical tunneling phenomenon [3] are promising candidate for beyond MOSFET devices. This dissertation addresses some of the simulation and modeling challenges for TFETs.

1.2. Problem Description

Advances in computational nano-electronics have facilitated atomic level simulation of non-conventional devices including TFETs as by J. Kang et al. [5] and M. Luisier et al. [6] in ballistic limit. Device-circuit and device-system co-design efforts have tried to address some of the issues with novel devices. For example Y. Lee et al. [7] used modified SRAM cell for TFET based memories and L. Jing et al. [8] employed extended read cycle for reliable functioning of novel spin based memory devices. Another aspect of interest is how these circuits and systems would behave in presence of unavoidable fabrication defects. Atomic simulations to study effect of defects like Line Edge Roughness (LER) in Graphene Nanoribbon (GNR) transistors have been carried out

by M. Luisier et al. [6]. These simulations are expensive in terms of time and memory. Calculating current for a 16nm GNR transistor at a given V_{DS} and V_{GS} can easily run into hours. Studying statistical effect of defects requires large number of such simulations.

We propose a filtering mechanism that can predict TFET devices which are severely defected – in the sense their I-V characteristic if calculated would be unacceptable. This would help to separate severely defected devices from the pool of defected devices under study and save valuable time and computational power. Our approach is to do a bandstructure analysis, for channel region with periodic boundary conditions and find effective bandgap. This bandgap when compared to ideal device tells us how bad it is in comparison to ideal device. Bandstructure analysis based on Tight Binding (TB) nearest neighbor model are much faster than calculation of I-V curve which requires self-consistent solution of Schrodinger's and Poisson's equation, this results in speed up [9].

We also implemented a compact model that can be used for circuit simulation for GNR TFET based on tunneling phenomenon in 1D [3] and Landauer's formula for ballistic current flow [9].

1.3. Organization of Thesis

This thesis is organized as follows. Chapter 2 explains advantages of 2D materials in dealing with short channel effects and justifies our choice of graphene as channel material. Chapter 3 describes qualitative operation of TFETs and mentions their advantages and disadvantages. Chapter 4 introduces semi-classical picture of current flow suitable for nano-devices. It also presents non-equilibrium Green's function method for

current flow. Device structure used in our study is also described in this chapter. Chapter 5 begins with introduction to Schrodinger equation and finally explains how we use it to derive bandstructure of GNR. The bandstructure analysis and results are mentioned in this chapter. Use of analytical expression for modeling current-voltage characteristics of TFETs are presented in chapter 6. Finally chapter 7 summarizes the work and suggests future work to be done.

2. 2D Materials and Graphene

2.1. Towards Quantum Capacitance Limit

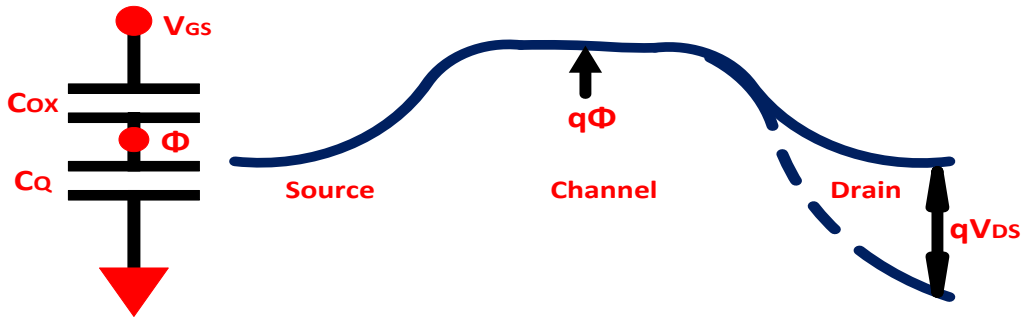

Figure 2. Quantum capacitance and channel potential

The actual gate capacitance C_G of a MOS device is series combination of gate oxide capacitance C_{OX} and inversion layer capacitance C_Q also called Quantum Capacitance as described by J. Knoch et al. [10] (fig. 2). Let ø be the potential maximum in channel. Then from fig. 2.

$$ø = \frac{C_{OX}}{C_{OX}+C_Q} V_{GS} \tag{3}$$

and

$$\delta ø = \frac{C_{OX}}{C_{OX}+C_Q} \delta V_{GS} \tag{4}$$

Ideally we would want channel potential to be controlled by gate potential 1:1, that is $\delta ø = \delta V_{GS}$, this requires $C_{OX} >> C_Q$. However in MOS devices with 3D channel material this condition is generally not satisfied and hence $\delta ø < \delta V_{GS}$. This results in increase in sub-threshold slope from its ideal value of 60mV/decade. In order to have ideal sub-threshold slope and more generally better gate control C_Q must be reduced such that C_{OX}

>> C_Q. C_Q is proportional to Density of States (DOS) in the channel. DOS is defined as number of allowed atomic states per interval of energy. In atomically thin 2D materials DOS is significantly lower than 3D materials resulting in much smaller C_Q and hence C_{OX} >> C_Q. This situation is called Quantum Capacitance Limit (QCL). Devices operating in QCL have better control over channel and hence lesser short channel effects and more ideal sub-threshold slope. Thus 2D materials like graphene and molybdenum disulphide (MOS_2) are better suited for low power and short channel devices due to their possibility of operation in QCL.

2.2. Graphene

2010 Noble Prize in Physics was awarded to Andre Geim and Konstantin Novoselov for isolation of single layer of carbon atoms through mechanical exfoliation technique commonly known as graphene [11]. Graphene has very high intrinsic mobility, very small effective mass, mean free path of micrometers. High intrinsic mobility and large mean free path makes it ideal material for realization of ballistic transistors. Also as mentioned in Section 2.1, its 2D form factors can help device operation in QCL and counter short channel effects.

However, graphene is a semimetal with zero bandgap which restricts its use in digital application. Bandgap engineering of graphene has been a wide area of research. Bandgap can be induced in graphene by drawing it into narrow ribbons as described by Y. Woo et al. [12] (fig. 3). A nanoribbon is more like a 1D structure and associated quantum confinement results in a bandgap.

Graphene Nanoribbon (GNR) can be of two types based on the arrangement of

edge atoms. Fig. 3 (a) shows an armchair GNR and fig. 3 (b) shows a zigzag GNR. Armchair GNRs are semiconducting since they have a bandgap whereas zigzag GNRs are metallic and devoid of any bandgap. It is these armchair GNRs that are useful for digital applications. GNRs are classified by number of dimer lines (*N*) along its width. A GNR is called *N*-GNR where *N* indicates number of dimer lines. A 11-armchair GNR is shown in fig. 3 (a) and a 6-zigzag GNR is shown in fig. 3 (b). Armchair GNRs with $N=3p+1$ and $N=3p$, where p is an integer, are semiconducting while those with $N=3p+2$ are metallic. This is shown in fig. 4 [12], it also shows that the bandgap of armchair GNR is inversely proportional to its width.

The dependence of bandgap on width has advantages and disadvantages. A. Raychowdhury et al. [13] used the geometry dependence of bandgap and hence threshold voltage of Carbon Nano Tubes (CNT) for multi valued circuit design. Similar circuits can also be implemented exploiting bandgap dependence of width for graphene. From a variation point of view this dependence isn't desirable. Line Edge Roughness (LER) are inevitable in fabrication of such GNR based devices, which means LER would affect the ideal bandgap and devices like TFETs which rely heavily on alignment of band profile of source, drain and channel can show unacceptable current-voltage characteristics in presence of LER.

The very study of such variations poses challenge given the amount of time needed for simulation. Also note there are other factors like non-idealities in fabrication of a single layer; that is the case where some regions in channel might be two or three layers instead of one. Simulation study of these non-idealities is essential and we present an

approach to speed up such simulations in chapter 5.

Our choice of graphene as study material was motivated by the fact that there has been lot of simulation study on graphene based devices and on devices with LER which could be used for comparing results of our simulation like those of M. Luisier et al. [6]. Also graphene has a simple structure with just one type of atoms i.e. Carbon as opposed to other 2D materials like MOS_2. This helps to make simulation faster. Semi- empirical parameters for graphene has been well established, this aspect is discussed in chapter 5.

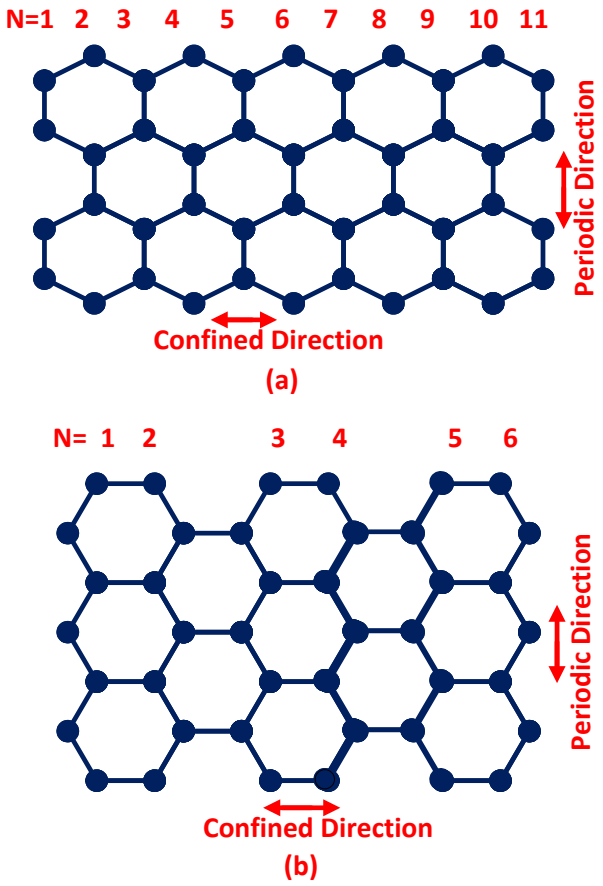

Figure 3. (a) 11- armchair GNR, (b) 6-zigzag GNR

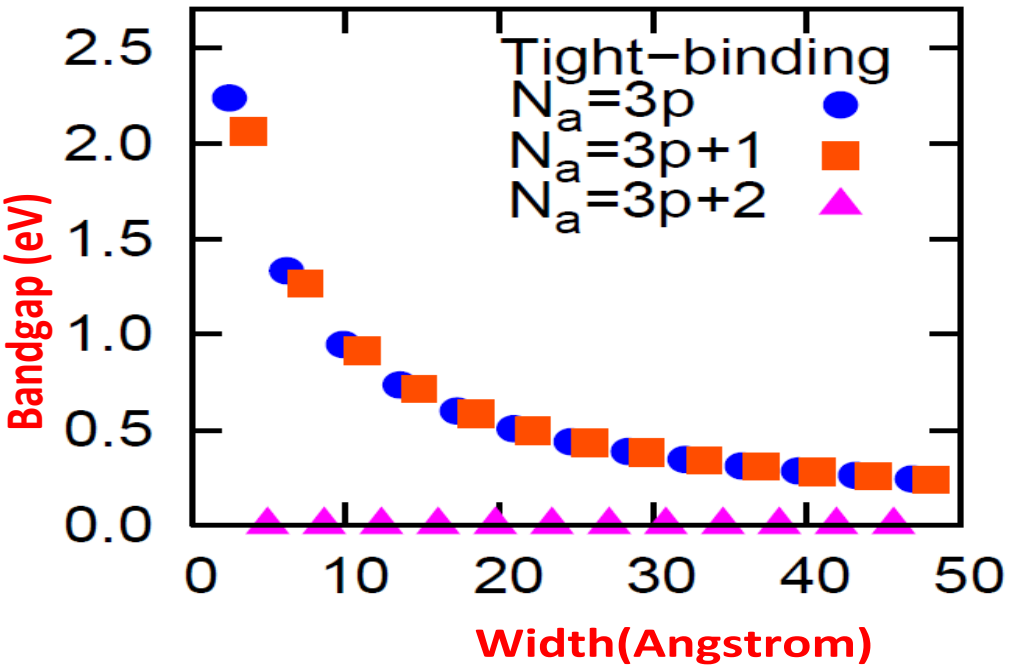

Figure 4. Bandgap versus width for armchair GNR using Tight Binding Model [12]

3. Tunnel FETs

3.1. Qualitative Operation of TFETs

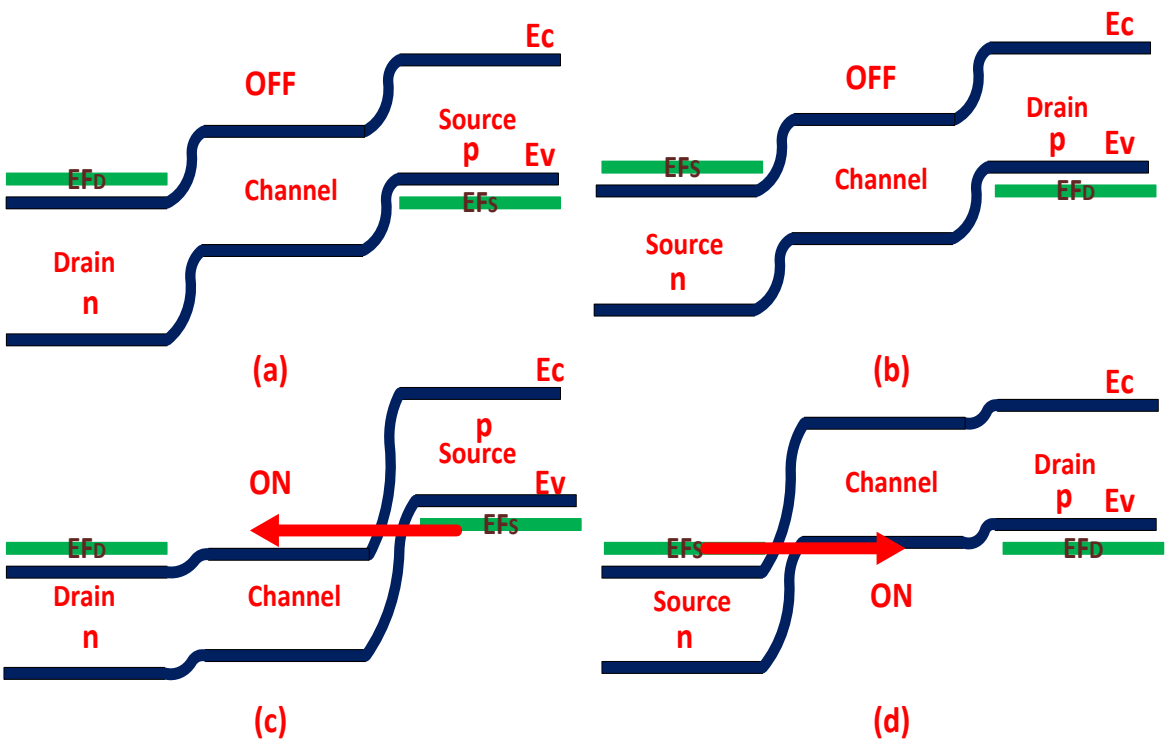

Figure 5. Band diagram for TFETs. (a) and (c) are nTFETs, (b) and (d) are pTFETs. (a) and (b) for VGS = 0. (c) and (d) for finite VGS

As discussed in Chapter 1, Tunnel FETs (TFETs) depend on quantum mechanical tunneling and hence do not have the theoretical limit of 60mV/decade for subthreshold slope as in MOSFETs based on thermionic emission. TFETs are *p-i-n* structures where 'p' indicates degenerately doped p-type semiconductor, 'n' is degenerately doped n-type semiconductor and 'i' is channel material which can be silicon as in conventional MOSFETs, nanowires, CNTs, graphene etc. Qualitative operation of TFET can be

understood by looking at their band diagram (fig. 5). Both p-type and n-type TFETs have same structure and are differentiated by the polarity of V_{GS} that makes device *ON*. Also the role of source and drain gets interchanged from pTFETS to nTFETS. Band diagrams for both *ON* and *OFF* state are shown for n-TFETs (fig. 5 (d) and (c)) and p-TFETs (fig. 5 (b) and (a) respectively). Green lines in source and drain region indicate respective Fermi levels (EF_S and EF_D). Almost all atomic states below Fermi level are filled and those above them are empty. In absence of V_{GS}, electrons in source see a rectangular potential barrier which is large enough to allow only very small sub-threshold current to flow (fig. 5 (a) and (b)). On the other hand when V_{GS} is applied the tunneling barrier reduces in size and electrons tunnel from source to drain giving a high *ON* current (fig. 5 (c) and (d)). For tunneling following conditions must be satisfied [3]

1. There must be occupied energy states on one side, from which electrons tunnel.
2. Tunneling barrier must be short and its height must be low.
3. Unoccupied states exist on other side at same energy level.

For TFETs in fig. 5, these conditions are satisfied only when the conduction band of channel goes below valence band of source, in nTFET. Electrons can now tunnel from source to channel constituting a current in presence of V_{DS}.

Current in nano-transistors operating in near ballistic limit is given by Landauer's equation [9]

$$I = \left(\frac{2q}{h}\right) \int_{-\infty}^{+\infty} dE.T(E)[f_o(E - \mu_1) - f_o\,(E - \mu_2)] \tag{5}$$

$$f_o(E) = \frac{1}{1+\exp[\frac{(E)}{kT}]} \tag{6}$$

Where q is electronic charge, h is Planck's constant, $T(E)$ is transmission and is function of energy E, f_o is Fermi function and μ_1 and μ_2 are Fermi level of source and drain respectively. For the case of TFETs $T(E)$ can be considered as transmission probability of electrons in source tunneling to channel region. It is possible to get compact analytical expression for $T(E)$ under 1D approximation, which would be discussed in chapter 6.

3.2. Challenges with TFETs

The most important aspect of tunnel FET is its possibility of very steep sub-threshold slope and hence its applications in low power circuits and systems. However there are issues associated with them. Firstly, TFETs have *ON* currents which are smaller than conventional MOSFETs, this is mainly due to the fact that TFETs are tunneling based devices as opposed to MOSFETs which gives higher current. This low *ON* current especially in presence of wire parasitics turn out to be the limiting factor for circuit performance as shown by N. Mojumder et al. [14]. Moreover TFETs are unidirectional devices, that is source and drain in TFETs are fixed as opposed to MOSFETs where they are interchangeable. This interchangeability of source and drain for MOSFETs allows their use as access transistors in SRAM cells. Nevertheless, attempts have been made by Y. Lee et al. etc. on circuit level to use modified SRAM cell that can operate with TFET devices [7].

Despite these challenges TFETs have been an active area of research and a number of groups have fabricated TFETs based on various channel material. A. Seabaugh et al. [4] have provided a good review of such TFETs.

4. Quantum Simulation and GNR-TFET under Study

4.1. Current flow: Semi-Classical Perspective

It has been believed classically that resistance arises because of collisions of electrons (with electrons or atoms) in a conductor during its passage from one terminal to another. This picture quickly vanishes if we consider a very small conductor where electrons travel from one end to another without collisions called as ballistic transport. In fact one may even ask if it makes sense to talk in terms of resistance and hence conductivity of ballistic devices. [9] provides excellent description of current flow at quantum level. One can understand the flow of current in ballistic nano-devices through fig. 6. Device in fig. 6 consists of three regions – source, channel, drain. Each of these regions has number of atomic states that can hold one electron (2 if spin included) each. Source and drain are equilibrium reservoirs, having continuous atomic states without any bandgap, characterized only by their Fermi levels, μ_1 and μ_2 respectively. Note, most states above Fermi level are devoid of electrons and those below them are filled of electrons. On application of V_{DS}, Fermi levels of source and drain move apart by an amount V_{DS} as shown in fig. 6. Let's assume the channel region has just one atomic state. In case of real devices like GNR TFETs channel would have continuous atomic states with bandgap in between. If this atomic state lies in between the Fermi levels of source and drain then, the source keeps pumping electrons into channel to attain equilibrium with it while the drain keeps pulling out to establish equilibrium between itself and channel. This results in a net flow of current.

If $\frac{\gamma 1}{\check{h}}$ and $\frac{\gamma 2}{\check{h}}$ are the rate at which electrons in channel will escape to source and drain respectively, then current through the device considering one atomic state in channel is given by [9]

$$I = \frac{2q}{\check{h}} \frac{\gamma 1.\gamma 2}{\gamma 1 + \gamma 2} [f_1 - f_2]$$

Where q is electronic charge, $\check{h}$ is modified Planck's constant, f_1, f_2 are source and drain Fermi functions respectively. This equation can be extended to devices where channel has many atomic states and the current in those devices is given by an integral equation which takes care of all atomic states in channel by integrating energy from $-\infty$ to $+\infty$.

$$I = \left(\frac{2q}{h}\right) \int_{-\infty}^{+\infty} dE.T(E)[f_o(E - \mu_1) - f_o\,(E - \mu_2)] \quad (7)$$

$$f_o(E) = \frac{1}{1+\exp[\frac{(E)}{kT}]} \quad (8)$$

Where *T(E)* is transmission and is function of energy *E*, f_o is Fermi function and μ_1 and μ_2 are Fermi level of source and drain respectively.

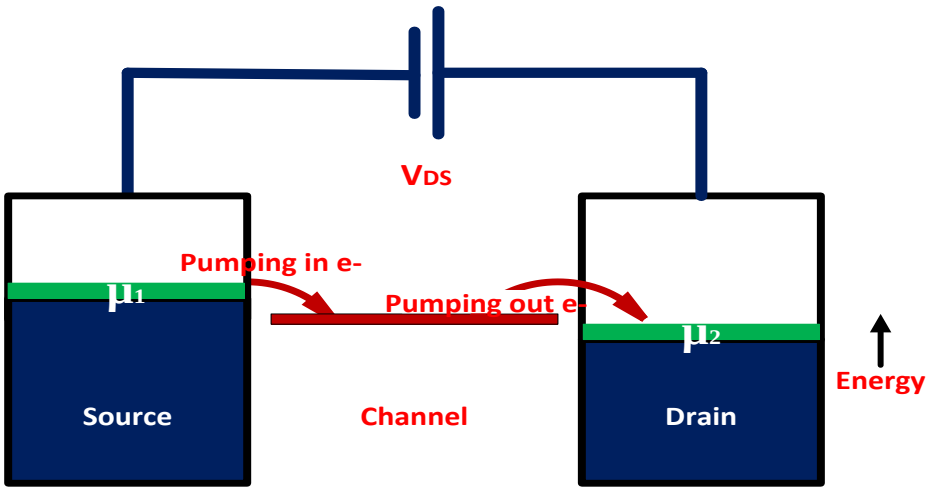

Figure 6. Semi-classical picture of current flow in nano-devices. Shaded regions in source and drain indicate states with filled electrons. Channel has one energy level as shown.

4.2. NEGF Approach for Nano-Device Simulations

From equation (7), we see the only unknown quantity we need for calculating current for a device with arbitrary channel material is transmission function *T(E)*. Non Equilibrium Greens Function (NEGF) formalism provides a well defined way for calculating *T(E).* It has been detailed by S. Datta et al. [9]. Following matrix equations illustrate calculation of *T(E)*

$$G(E) = [(E + i0^{+})I - H - U_L - U_{other} - \sum_1 - \sum_2]^{-1} \quad (9)$$

$$\Gamma_1(E) = (\sum_1 - \sum_1{}^{\dagger}) \text{ an} \Gamma_2(E) = (\sum_2 - \sum_2{}^{\dagger})\text{d} \quad (10)$$

$$T(E) = trace(\Gamma_1 G \Gamma_2 G^{\dagger}) \quad (11)$$

One can also calculate electron density *(N)* in the channel by using following equation.

$$N = G[\Gamma_1 f_1 + \Gamma_2 f_2]G^{\dagger} \quad (12)$$

Where *G(E)* is retarded Green's function, *E* is energy, *i* is square root of -1, 0^{+} is infinitesimal quantity greater than 0, *H* is Hamiltonian matrix, U_L is Laplace potential and can be viewed as potential drop across device due to V_{DS}, U_{other} can be viewed as potential on gate terminal, $\sum_1$ and $\sum_2$ are self-energy matrices for source and drain respectively; they define coupling of channel to source and drain. A superscript '†' indicates conjugate transpose of a matrix. *f1* and *f2* are Fermi functions.

The derivation of these equations requires concepts from quantum mechanics and linear algebra. We however are interested only to know how to implement these in a computing tool like Matlab® or Scilab®. For a given channel region with *N* atoms *H* is *N*x*N* matrix assuming one basis function for each unit cell. How to write *H* for GNR will be discussed in chapter 6.

A pseudo code for implementing the equations (9)-(12) is shown below. The code structure follows closely to that used by H. Raza et al. [15].

```
E_from = -1.1                    // Decides starting value for range of energies.
E_to = 3.1                       // Decides ending value for range of energies.
EE= E_from:0.1*KT:E_to           // EE = energy range in steps of 0.1 *KT
NE=length(EE)                    // length of range of EE

for kE = 1:NE                    // For every energy value in EE(kE)
   E=EE(kE)                      //Current energy = EE(kE)

   Sig1 =zeros(Nd,Nd),           //Defining self energy matrices
   Sig2 = Sigma1
   Sig1(1,1)= -to*exp(i*ka1)     // [9]
   Sig2(Nd,Nd) = -to*exp(i*ka2)

   Gam1 = i*(Sig1-Sig1')         //Equation (10)
   Gam2 = i*(Sig2-Sig2')         //Equation (10)

   G=inv((E+i*1e-6)*eye(Nd,Nd)- H -Sigma1 - Sigma2)  //Equation (9)

  TT(kE)=trace(Gamma1*G*Gamma2*G')    // Transmission calculation. Equation (11)

end
```

From equations (9)-(12) we can see *G(E)* depends on *U (U= U_L + U_{other})* and electron density *N* depends on *G(E)*. Electron density however must also satisfy Poisson's equation given by [16]

$$\nabla.(\epsilon\nabla U) = q^2[N_D - N] \tag{13}$$

Where ∇ is divergence operator, ϵ is permittivity, q is electronic charge, N_D is electron density due to ionized atoms. Thus equations (9), (10), (12) and equation (13) must be solved self consistently. Once a self consistent state is reached transmission can be

calculated by equation (11). Attaining this self-consistency increases the time required for simulation of a given device.

4.3. ATK Simulation Flow

ATK stands for Atomistic Tool Kit [16] and is a simulation tool that can calculate properties of a nano-system including current through transistor devices. We used ATK as the simulation tool for simulating GNR-TFET devices with and without defects. This section gives a short introduction on simulation flow used in ATK.

The first step is to define a device structure. As mentioned earlier a device is composed of three regions contact-1 (source), contact-2 (drain) and channel (scattering region). Parameters to be decided for channel regions include channel length (L), channel (W), material of channel. A gate and dielectric region has to be included which requires decision on parameters like dielectric constant, dielectric thickness, gate length.

Once the device geometry is fixed, ATK provides three ways to calculate the Hamiltonian matrix (H). These are Density Functional Theory (DFT), ATK – Extended Huckel Model and ATK - Slater Koster Model. DFT is more like first principle calculation and has not been used in our study. ATK- Extended Huckel Model described by K. Stokbro et al. [18] and ATK – Slater Koster Model as developed by M. Elstner et al. [19] are parameterized models where parameters are fixed such that the results match more rigorous calculations like those of DFT. Hence such parameterized models are called semi-empirical models. Important parameters to be selected once simulation model is fixed are –

1. Electrode parameters that include electrode voltage, electrode temperature and

charge on electrode. (Note electrode charge can be used to effectively dope an electrode with *n* or *p* type.)

2. Poisson equation solver (see equation (13)) algorithm which can be Fast Fourier Transform (FFT), 2D- FFT and multi grid.
3. Boundary conditions. These are for channel region which can be Neumann or Dirichlet condition. Neumann condition says electric field at boundary is zero whereas Dirichlet condition says voltage at the boundary is equal to some designated voltage.
4. Brillouin zone sampling (*k* point sampling).

How these parameters were selected would be discussed in section 4.4. These parameters and other important parameters are shown in fig. 7. A through explanation for each of these parameters can be found in [16].

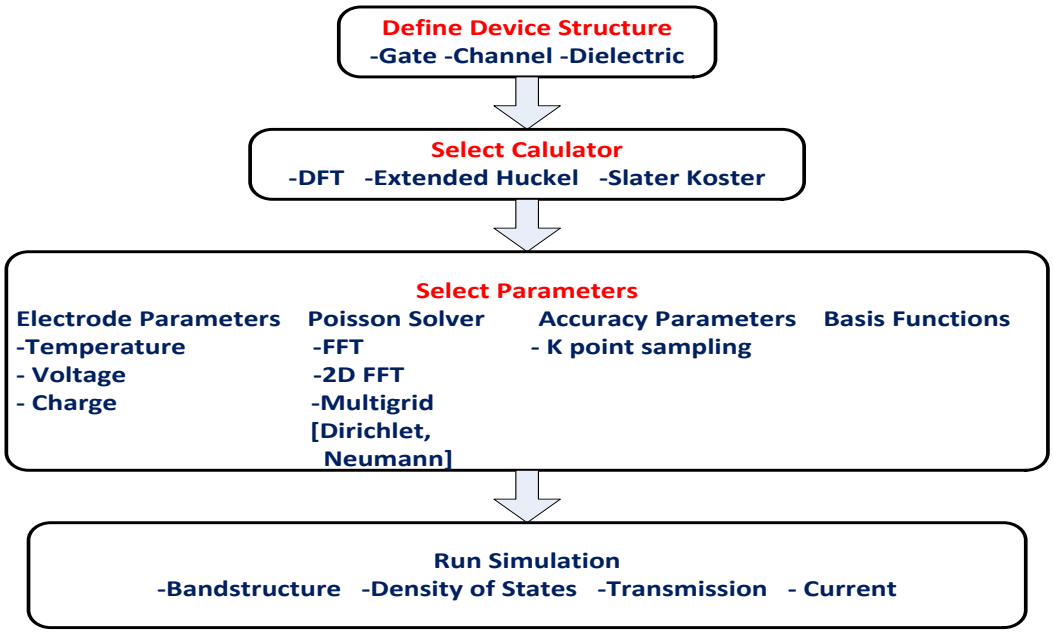

Figure 7. Simulation flow in ATK

4.4. Device Architecture and Simulation

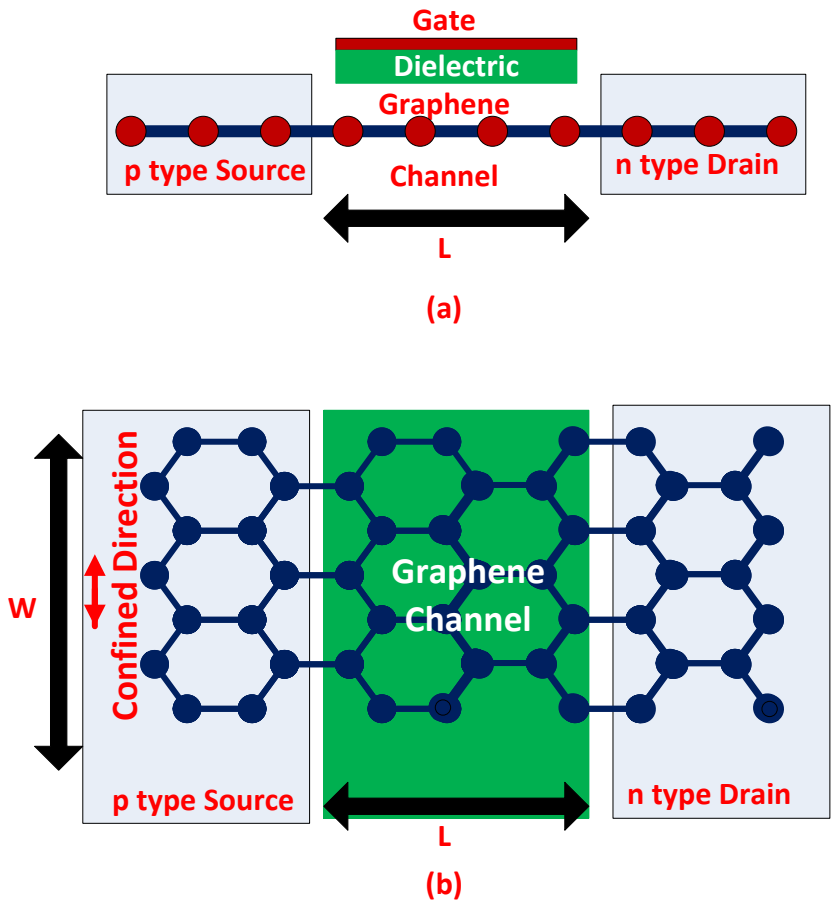

Figure 8. Device structure used for simulation. Note edge-passivation not shown

The device architecture used in our simulation is shown in fig. 8. The source, drain and channel region all are made of GNR with 21 dimer lines passivated with hydrogen atoms to take care of dangling bonds (not shown in figure). The source and drain must be doped to get a *p-i-n* like structure as in fig. 5. This was accomplished by adding some positive charge of 0.0002 electrons in drain and a negative charge of 0.0002 electrons in source region. The dielectric constant was set to be 4. The device length was 16nm.

The *k* point sampling was set to 1x1x50. Multi-grid Poisson's solver was selected with Neumann boundary condition in *X*, *Y* direction (normal to transport directions) and Dirichlet condition in *Z* direction (direction of current flow). V_{GS} was swept from -1.5V to 1V under a V_{DS} of value 0.8V. Energy range for transmission calculation was selected in the range of -3eV to 3eV. The simulated I_D - V_{GS} curve is shown in fig. 9.

The ideal sub-threshold slope for a MOSFET like device (60mV/decade) is also plotted on same graph. One can see that TFETs offer less that 60mV/decade and hence are of paramount interest for low power circuits and systems.

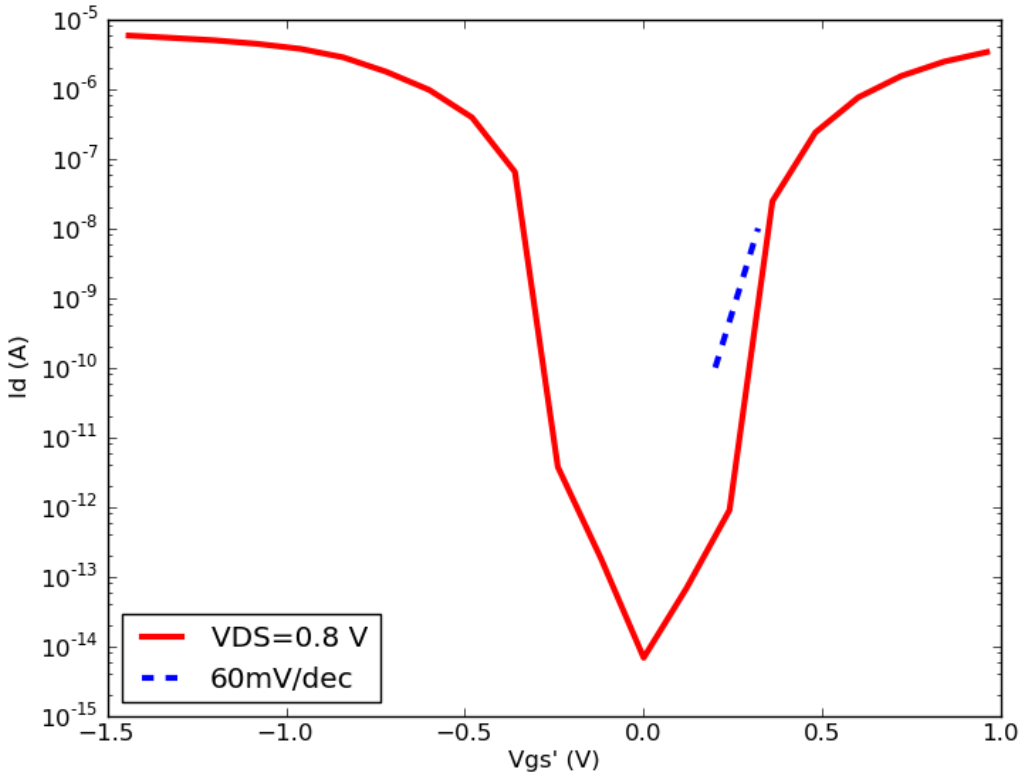

Figure 9. I_D versus V_{GS} curve generated using ATK for a device size with channel length of 16nm. Note $V_{GS'}$ on horizontal axis is assumed to be effective V_{GS} including metal work function

5. Speeding-up Defect Analysis

5.1 Schrodinger Equation and Basis Functions

It has been known that electrons in an atom or a device consisting of many atoms can only occupy certain discrete levels of energy. The transmission function mentioned in chapter 4 is a function of density of these states (per unit energy) and velocity associated with them. The starting point to calculate this transmission function or density of states is Schrodinger equation. The time independent form of Schrodinger equation can be written as

$$E\Psi = (-\frac{\hbar^2}{2m}\nabla^2 + U)\Psi \tag{14}$$

Where ħ is modified Planck's constant, m is mass of electron, ∇ is divergence operator, U is potential and Ψ is eigenfunction. The eigenvalues E of equation (13) specifies energy states an electron can occupy when bounded in a potential given by U. The operator $(-\frac{\hbar^2}{2m}\nabla^2 + U)$ is termed as H, the Hamiltonian operator that appeared in the NEGF formalism in chapter 4.

To start from equation (10) and calculate transmission function and hence current voltage characteristic following NEGF equations is a time consuming and computationally intensive task. We exploit the fact that calculation of bandstructure by suitable approximation of equation (14) is much faster and gives us an idea of the bandgap of structure under study (including defects). Comparison of the calculated bandgap (for devices with defect) with ideal bandgap (device without defects) will tell us how near the device is to ideal device and can be used as a means to filter out bad

devices.

Bandstructure is a plot of various energy states an electron is allowed to have based on Schrodinger equation. For our device of interest these states form a quasi-continuous band with gaps in between known as bandgaps. To proceed with the bandstructure calculation of a structure the first step is to select a set of basis functions.

For example, we know that hydrogen atom has one electron in a spherically symmetrical energy states called 1s. If we were to calculated the bandstrcuture of a hydrogen molecule one can select two 1s orbital each centered on each hydrogen atom as basis functions. The resulting atomic state to be calculated, that is the atomic state for a hydrogen molecule can then be thought of as superposition of these two basis function. In general, if Ψ is the function we are looking for, we can express it as superposition of basis function $\phi_m$with weights u_m [9].

$$\Psi(r) = \sum_{m=1}^{M} \phi_m u_m(r) \tag{15}$$

Where *r* is position vector. Substituting equation (15) into equation (14) we can obtain the matrix form of Schrodinger equation given by

$$E[S]\{\phi\} = [H]\{\phi\} \tag{16}$$

Where *H*, *S* are *Nb*x*Nb* matrix where *N* is number of atoms and *b* is number of basis function per atom. $\{\phi\}$ is column vector which gives weight of basis functions $u_m(r)$.

Matrix elements of *S* and *H* are given by

$$S_{nm} = \int dr u_n^*(r) u_m(r) \tag{17}$$

$$H_{nm} = \int dr u_n^*(r) H_{op} u_m(r) \tag{18}$$

Where H_{op} is $(-\frac{\hbar^2}{2m}\nabla^2 + U)$. Once we have *H* and *S* matrix equation (16) can be solved to get allowed values of *E*. These allowed values when plotted results in bandstrcuture.

5.2. Nearest Neighbor Tight Binding Semi-empirical Method

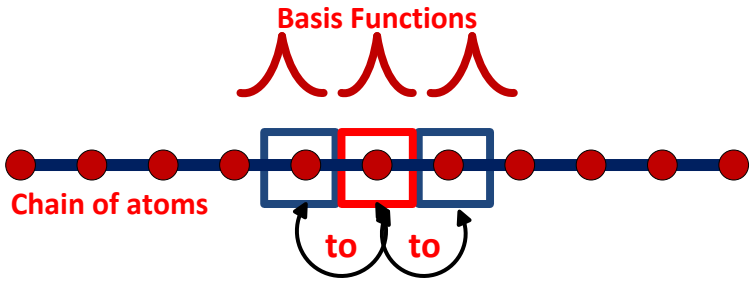

Figure 10. System consisting of chain of atoms. Each atom interacts only with its nearest neighbor.

Consider a chain of atoms as shown in fig. 10. In order to calculate the bandstructure for this hypothetical material using equations (16)-(18), we start by selecting a set of basis functions. Let the basis functions be as shown in fig. 10 (used only for illustration purpose) [20]. Consider *Hnn*, as per equation (18), we would get some number after performing the integral. Let that number be **ϵ**. Thus all *Hnn* that is *H11*, *H22* etc. will be **ϵ**. Before going to off diagonal elements of *H* that is *Hnm* when *n* is not equal to *m* we make an important assumption called the nearest neighbor assumption.

Nearest neighbor assumption says that the given atom only interacts with its nearest neighbor atom all other interactions are ignored. Thus in fig. 10, the atom in center box interacts with the two boxes beside it all other interactions are zero. This means only those elements of *H* are non-zero where *m=n+1 or n-1*. Since *n+1* and *n-1* atoms are equidistant from atom *n*, the integral in equation (18) will evaluate to same number, let us

call it t_o. Thus H turns out to be a tri-diagonal matrix where the diagonal elements are ϵ and the upper and lower diagonal elements are t_o. H would look like

$$H=\begin{bmatrix} \epsilon & to & 0 & 0 & 0 & 0 & 0 & 0 \\ to & \epsilon & to & 0 & 0 & 0 & 0 & 0 \\ 0 & to & \epsilon & to & 0 & 0 & 0 & 0 \\ 0 & 0 & to & \epsilon & to & 0 & 0 & 0 \\ 0 & 0 & 0 & to & \epsilon & to & 0 & 0 \\ 0 & 0 & 0 & 0 & to & \epsilon & to & 0 \\ 0 & 0 & 0 & 0 & 0 & to & \epsilon & to \\ 0 & 0 & 0 & 0 & 0 & 0 & to & \epsilon \end{bmatrix}$$

Thus to calculate H we have to perform number of integrals given by equation (18), in fact the methods where these integrals are explicitly calculated are called as first principle method and are major time consuming process. We can avoid calculation of any integrals and even calculation of S matrix by invoking a method called semi-empirical method. The H matrix shown above tells us there are two parameters ϵ and t_o which if known would make calculations of equation (18) needless. These parameters then can be considered as fitting parameters, which can be fitted to a first principle calculation and then used again and again without worrying about the integrals and even about choosing a set of basis function. In short all we want to know is which elements in H are non-zero and what values for those elements matches first principle calculations. Same is true for S matrix, however we can ignore the S matrix by the justification that the elements of H are decided empirically and we can choose them to match results even if S was an identity matrix. For example in graphene the carbon atoms are separated by a fixed distant, fitted value of ϵ and t_o for graphene are 0eV and -3eV respectively [21].

Hamiltonian H thus obtained via fitting parameters when fed to a computing tool like Matlab® or Scilab® can easily calculate the eigenvalues E, which gives the

bandstructure. The next section describes specific details for calculation of GNR bandstructure.

5.3. Nearest Neighbor *pz*-Orbital GNR Bandstructure

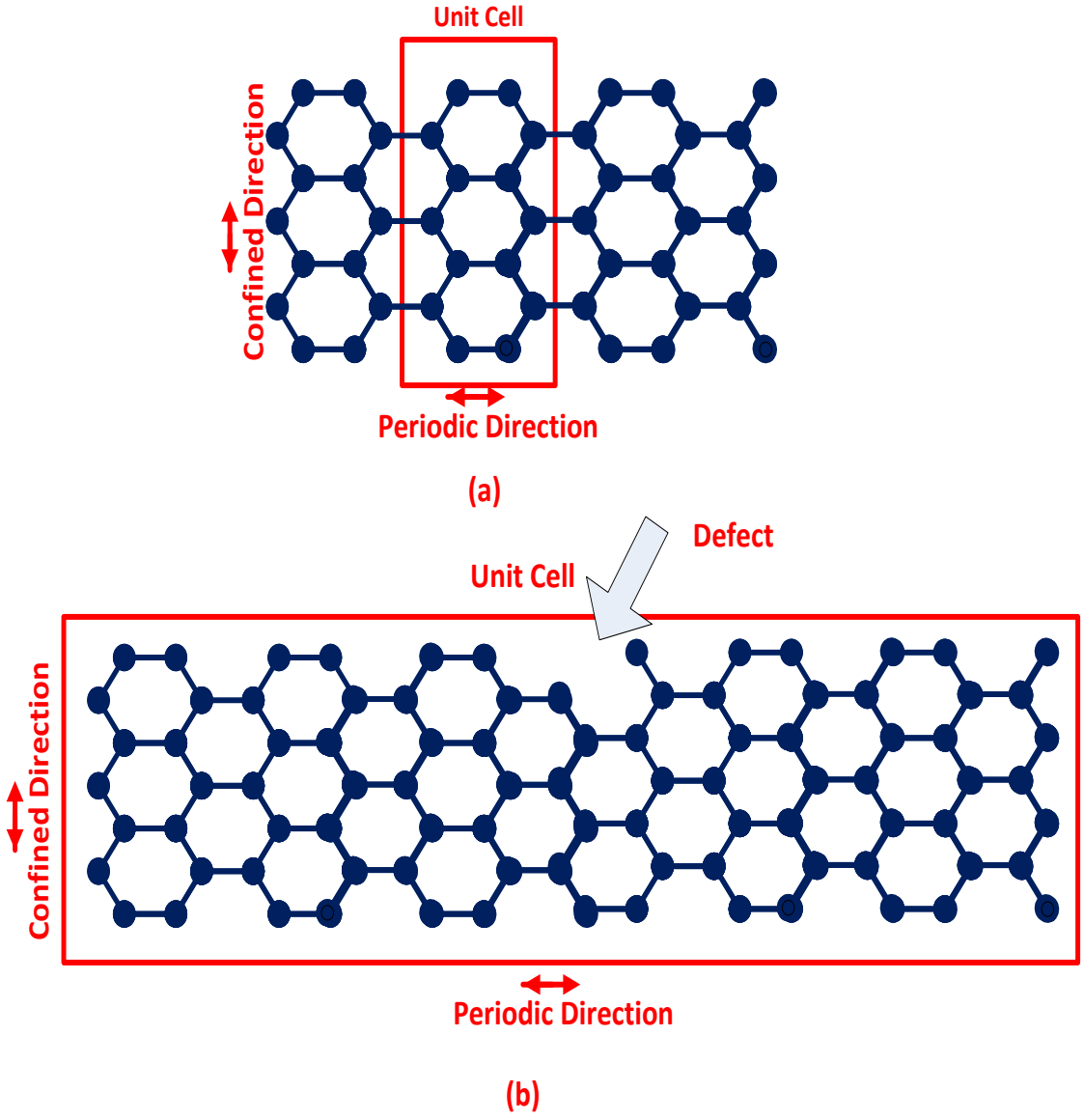

Figure 11. (a) A perfect GNR and its unit cell. (b) GNR with defect and its unit cell

Consider the GNR shown in figure 11 (a). Let us first select a unit cell such that when the unit cell is repeated we can reconstruct entire GNR. The unit cell is shown by a box. The GNR can now be considered as a 1D chain of unit cells as shown in figure 10. From equation (16) and ignoring S we have

$$E\{\phi\} = [H]\{\phi\} \tag{19}$$

Writing in terms of component of the matrix appearing in above equation we have [20]

$$E\phi_n = \sum_m H_{nm}\phi_m \tag{20}$$

Using the ansatz $\phi_n = \phi_0 e^{ikd_n}$ the above equation becomes

$$E = \sum_m H_{nm}\, e^{ikd_m - d_n} \tag{21}$$

Where *dn* and *dm* are position vectors with respect to arbitrary origin and *k* spans a range of 2л. Equation (21) is called principle of bandstructure and can be applied to calculate bandstructure of periodic solids.

Equation (21) cannot be used for GNR bandstructure calculation as it is since we have assumed *Hnm* to be a number in other words we have assumed one basis function per unit cell. For GNR as in figure 11 (a), there are 14 atoms in one unit cell which means there are 14 basis function per unit cell since for graphene we use a single *pz* orbital as basis function. Thus *Hnm* becomes a 14x14 matrix. In general if there are *b* basis functions per unit cell *Hnm* is a *b*x*b* matrix. Equation (21) then changes to

$$E\{\phi\}_0 = \sum_m [H]_{nm}\, e^{ikd_m - d_n}\{\phi\}_0 \tag{22}$$

Where *[H]nm* is now a matrix. Feeding equation (22) to Matlab will give us eigenvalues *E* for a selected value of *k*.

For taking into account, say a single defect as shown in figure 11 (b) we extend the

unit cell to include entire ribbon. The *[H]nm* matrix is now a *N*x*N* matrix where *N* is number of atoms in ribbon. Note for nearest neighbor assumption we have to consider *[H]nn, [H]n,n+1, [H]n,n-1* and use equation (22) to calculate eigenvalues.

Only those elements are non-zero that are connected to one another thorough a nearest neighbor interaction. As mention ϵ for GNR is 0eV and t_o is -3eV. A Scilab® script which sets up matrix *[H]nm* based on coordinates of carbon atom in GNR, implements equation (22), calculates eigenvalues and plots it versus k is given in appendix, section 9.1. Fig. 12 shows one such plot for armchair GNR with 10 dimer lines using the script.

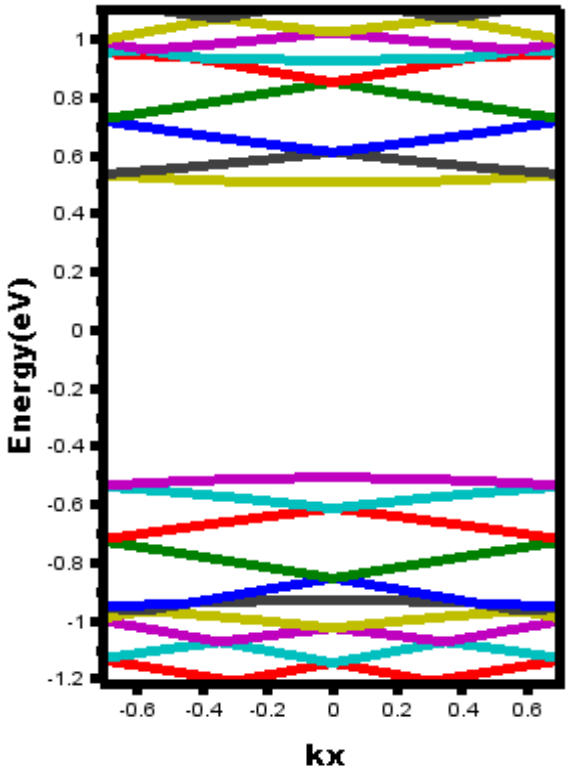

Figure 12. Bandstructure of armchair GNR with 10 dimer lines calculated through our script.

5.4. Results

We took an armchair GNR with 10 dimer lines and 100 atoms along edge. The device structure was same as in section 4.4. The kind of defect investigated was line edge roughness (LER), which implies absence of some edge atoms due to fabrication limitations. Probability of edge defect *p* was defined as number of missing edge atoms divided by total number of edge atoms. We generated 20 defected devices with *p* = 2%, 4%,8%,10%, 5 devices for each value of *p*. Edge atoms were randomly selected and deleted to introduce LER. Our bandstructure Scilab® script was used to calculate bandgap for each of these configurations. The calculated bandgap versus configuration number is shown in fig. 13. Note the first five devices are for =2%, next 5 for p=4% and so on.

Ideal bandgap for a device without LER is shown by a solid line. We see LER may severely affect the bandgap in fact many devices in fig. 13 fall below a bandgap of 0.2eV. Such devices with very low bandgap deviate lot from the ideal value; we would expect these *severely defected* devices to produce unacceptable current-voltage characteristics and hence we could altogether drop these devices from the pool of devices and save valuable time by not calculating I-V curves for them.

To verify that devices which are severely defected do produce unacceptable current-voltage characteristic we simulated all 20 configuration and calculated I-V curve for them. Fig. 14-17 shows current-voltage curve for all configurations. As expected devices with bandgap less than 0.2eV from fig. 13 show either very low *ON-OFF* current

ratio or exhibit unacceptable curves. Fig. 17 which is for devices with p=10%, almost all devices (except one) are severely defected. Thus one could conclude by looking just at fig. 13 that p=10% and further degradation must be avoided in fabrication and ways should be developed that most of manufactured ribbons fall below p=10% LER.

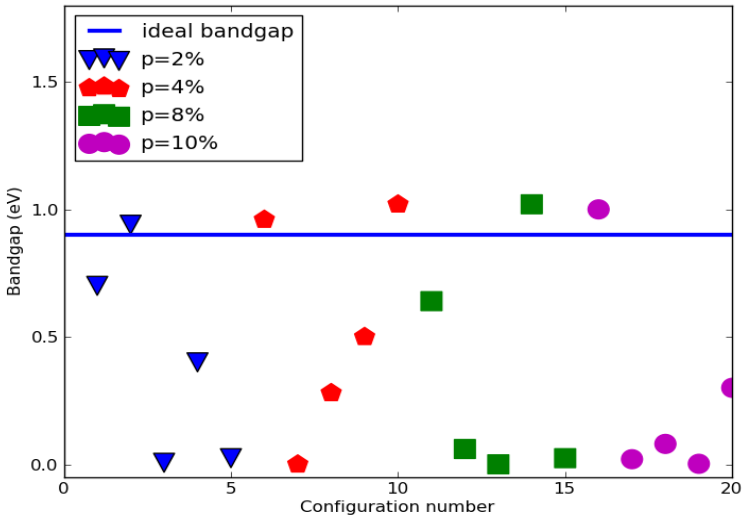

Figure 13. Calculated bandgap versus configuration number for defected devices.

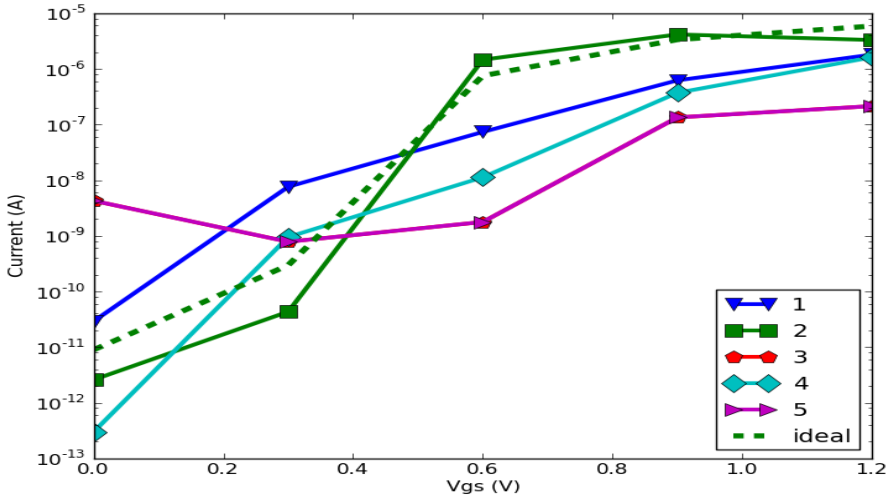

Figure 14. Current –voltage plot for all five device configurations 1-5, with p=2%

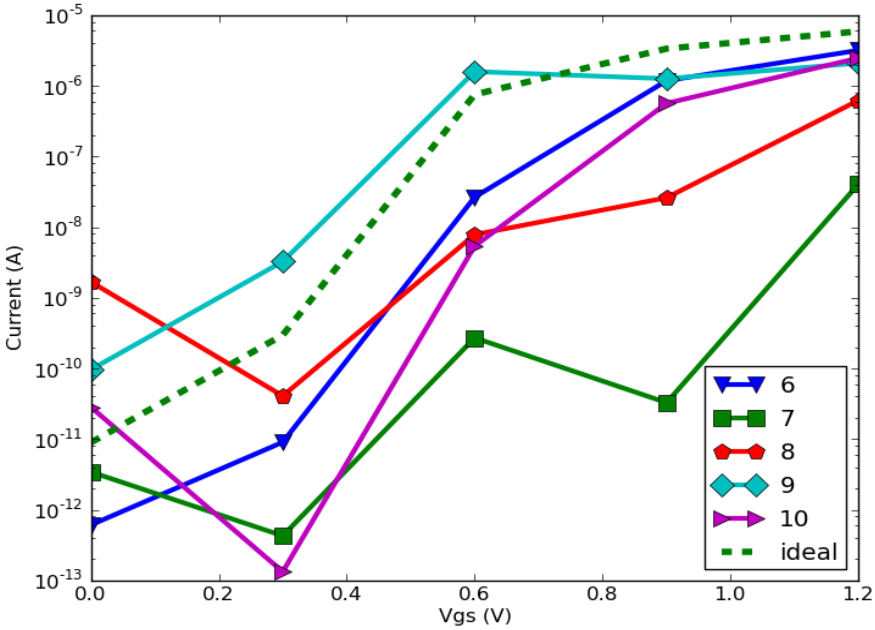

Figure 15. Current –voltage plot for all five device configurations 6-10, with p=4%

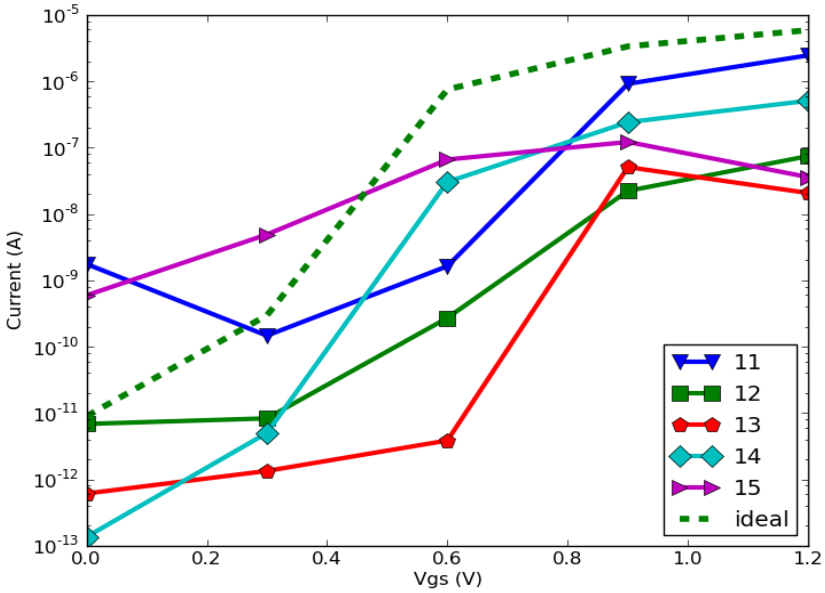

Figure 16. Current –voltage plot for all five device configurations 11-15, with p=8%

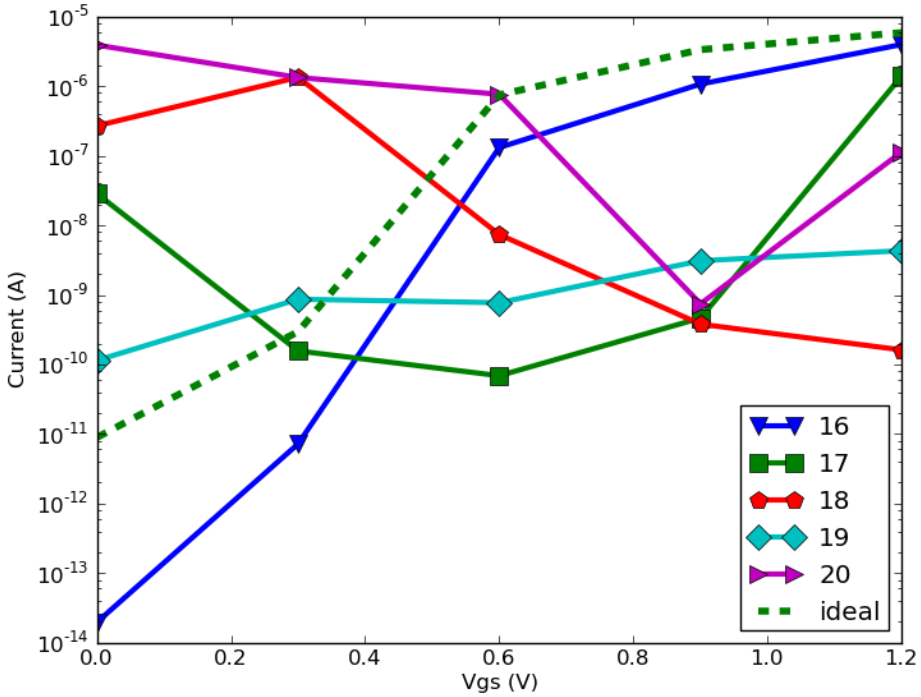

Figure 17. Current –voltage plot for all five device configurations 16-20, with p=10%

6. Compact Model for Current Voltage Relationship

6.1. Modeling I_{ON} and I_{OFF}

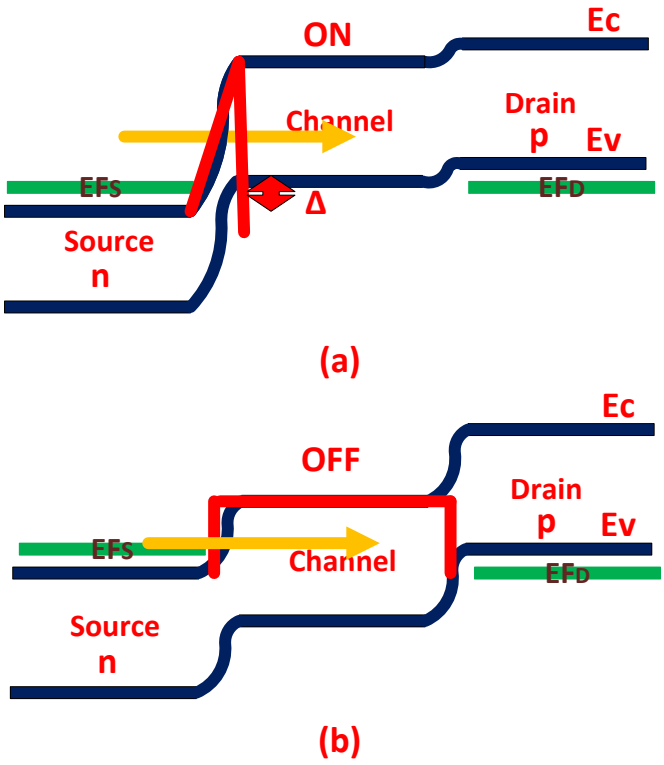

Figure 18. (a) Potential barrier profile for electrons in source in *ON* state. (b) Potential barrier profile for electrons in source in *OFF* state.

In order to investigate possible advantages and disadvantages of a novel device like GNR TFET on circuit and system level, it is important to have a compact SPICE model. Such SPICE models have been developed for wrap-around gate TFETs by N. Mojumder et al. [14]. Graphene FETs compact model including line edge roughness has been recently developed by Y. Chen [22]. [22] uses analytical expressions for sub-bands of GNR to model the device current. Variations are included by accounting for an effective

subband which is a weighted sum of a subband with *N* dimer lines and say *N-1* dimer lines.

We would rather go by semi-classical equations governing the mechanism of current flow in a TFET. Our model is developed on similar lines as by N. Mojumder et al. [14]. The advantage of such a model is its simplicity of derivation and its intuitiveness which vanishes quickly when more complicated quantum mechanical equations are used.

To model I_{ON} we start with equation (7), repeated here for convenience.

$$I = \left(\frac{2q}{h}\right) \int_{-\infty}^{+\infty} dE.T(E)[f_o(E - \mu_1) - f_o\,(E - \mu_2)] \tag{23}$$

$$f_o(E) = \frac{1}{1+\exp[\frac{(E)}{kT}]} \tag{24}$$

The only unknown function in equation (23) is *T(E)*. For a device in *ON* state fig. 18 (a), the potential profile seen by an electron in source can be approximated by a triangular potential barrier, marked in fig. 18 (a). This is very similar to the potential barrier encountered by carriers in a tunnel diode. For a triangular potential barrier one can approximation and derive an analytical expression for tunneling probability *T(E)*, which is given by [3]

$$T_{ON}(E) = \exp\left(\frac{-4\sqrt{2m^*}{E_G}^{3/2}\lambda}{3\hbar(E_G+\Delta)}\right) \tag{25}$$

Where m^* is effective mass of electron, E_G is bandgap of channel, λ is length scale over which potential changes and is called screening length, ħ is modified Planck's constant and Δ is energy window where tunneling takes place (figure 18 (a)).

Pulling *T(E)* outside integral in equation (23) and integrating it in energy range from Ec,source to Ev,channel using f_o as in equation (24) gives [14].

$$I_{ON} = \frac{2q}{\hbar} T_{ON} log_e \left| \frac{(1+e^{\frac{E_{diff}}{kT}})(1+e^{\frac{(E_{dop}-\Delta)}{kT}})}{(1+e^{\frac{E_{dop}}{kT}})(1+e^{\frac{(E_{diff}-\Delta)}{kT}})} \right| \quad (26)$$

$$E_{dop} = E_{F,source} - E_{c,source}$$

$$E_{diff} = E_{dop} + V_{bi} + q|V_{DS}|$$

V_{bi} is built-in potential for *p-i-n* structure.

Next we would model I_{OFF}. During *OFF* state current is constituted by direct source to drain tunneling as shown in figure 18 (b). Electrons in source now see a rectangular potential barrier marked in fig. 18 (b). The tunneling probability for electrons to tunnel through a rectangular potential barrier can again be derived and is given by [3]

$$T_{OFF}(E) = \exp\left(\frac{-2L\sqrt{2qm^* E_G}}{\hbar}\right) \quad (27)$$

We could use this T_{OFF} with equation (23) under suitable limits to get I_{OFF}, however there is a simpler way to deal with the integration. f_D - f_S, can be approximated by a triangle where f_D and f_S are Fermi function of drain and source respectively. Integral f_D - f_S is area under the curve which can be approximated by a triangle. The area of this triangle would be 0.5*1*(V_{DS} + V_{bi}). Thus the integral can be replaced by 0.5*1*(V_{DS} + V_{bi}) we add a scaling term k_s as a fitting parameter resulting in OFF current as

$$I_{OFF} = T_{OFF}.k_s.0.5.(|V_{DS} + V_{bi}|) \quad (28)$$

Equations (26) and (28) are derived for pTFET, however these can also be used for nTFET by correct sign relation between Δ and V_{GS}.

Curve fitting was done such that for chosen parameters in equations (26) and (28) followed simulated curve for I_D-V_{GS} for nTFET device of size. Fitting with V_{DS} was done

by empirically fitting curves for arbitrary values of V_{DS}, the V_{DS} then used in above equation was obtained from actual V_{DS} and curve fitted equation that produced new V_{DS} such that curves matched different V_{DS} values. Fig. 19 shows the simulated and model data points. Code for implementing this model is given in Appendix, section 9.2 which also mentions values of various parameters used for fitting.

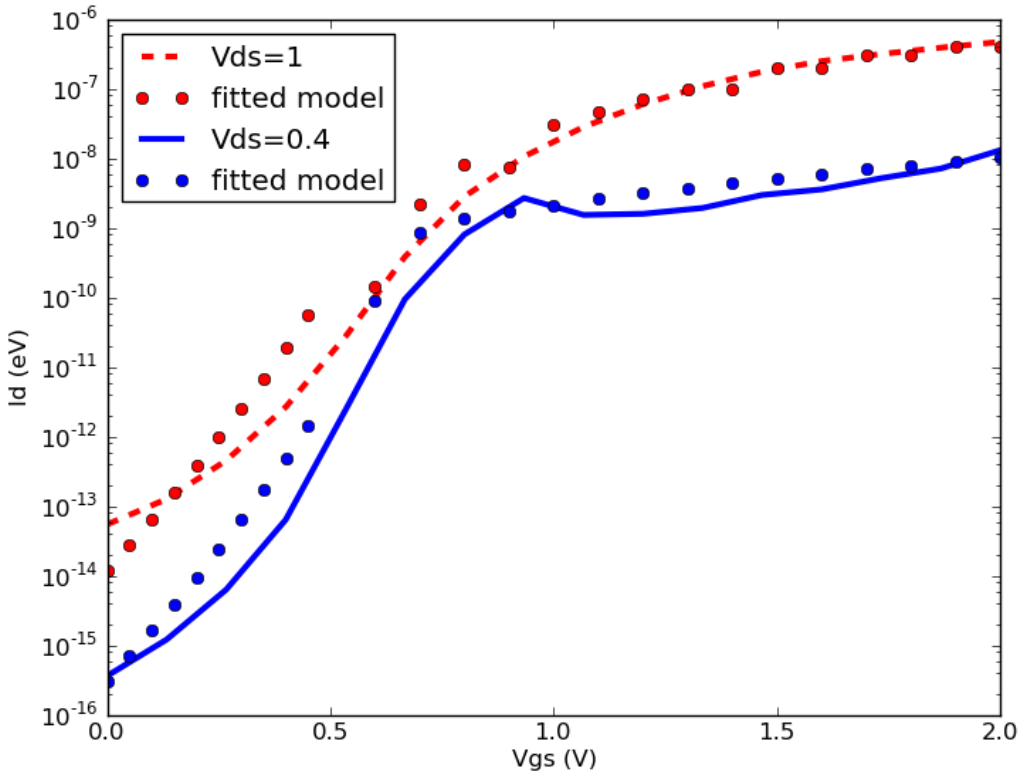

Fig. 19. Simulated and modeled data points for two different values of V_{DS}. Solid lines represent simulated data and dots correspond to model equations.

7. Conclusion and Future Work

We have developed a filtering mechanism that can be used as a speed-up technique for graphene based TFET devices with line edge roughness. Our method involves calculation of bandstructure which is much faster than calculating current-voltage characteristic and use the bandgap data from bandstructure to filter out those devices that can go for a full current-voltage simulation. Simulated devices show that the prediction of unacceptable devices based on bandstructure analysis matches with full-fledged current-voltage results.

We have also presented an analytical compact model for device current-voltage relationship. Such models can be used for circuit simulation.

Candidates for future work include use of our filtering method to study more complex system like monolayer MOS_2 based devices where one would be interested to know the effect on device performance if the channel consists of a mix of monolayer and multiple layers MOS_2.

On modeling side, the *OFF* current needs a more accurate representation including drain tunneling and impurity assisted tunneling. Modeling of variations in current-voltage curve with physics based or curve fitted parameters needs to be investigated. These variation models are necessary for example to do a Monte Carlo simulation of SRAM cells based on TFET devices.

8. References

[1] K. Roy, S. Mukhopadhyay, H. Mahmoodi-Meimand, "Leakage current mechanisms and leakage reduction techniques in deep-submicrometer CMOS circuits," *Proceedings of the IEEE* , Vol. 91, No. 2, pp. 305,327, Feb 2003.

[2] M. Lundstrom, Zhibin Ren, Datta Supriyo, "Essential physics of carrier transport in nanoscale MOSFETs," *Simulation of Semiconductor Processes and Devices, 2000. SISPAD 2000,* pp.1-5, 2000.

[3] S. M. Sze, K. N. Kwok, "*Physics of semiconductor devices*," John Wiley & Sons, third edition, 2006.

[4] A. C. Seabaugh, Q. Zhang, "Low-Voltage Tunnel Transistors for Beyond CMOS Logic," *Proceedings of the IEEE* , Vol. 98, No. 12, pp. 2095-2110, Dec. 2010.

[5] J. Kang, Y. He, J. Zhang, X. Yu, G. Ximeng, Z. Yu, "Modeling and simulation of uniaxial strain effects in armchair graphene nanoribbon tunneling field effect transistors," *Applied Physics Letters* , Vol. 96, No. 25, pp. 252105,252105-3, Jun 2010.

[6] M. Luisier, G. Klimeck, "Performance analysis of statistical samples of graphene nanoribbon tunneling transistors with line edge roughness," *Applied Physics Letters* , Vol. 94, No. 22, pp.223505,223505-3, Jun 2009.

[7] Y. Lee, D. Kim, J. Cai, I. Lauer, L. Chang, S. Koester, D. Blaauw, D. Sylvester, "Low-Power Circuit Analysis and Design Based on Heterojunction Tunneling Transistors (HETTs)," *Very Large Scale Integration (VLSI) Systems, IEEE Transactions on* , Vol. 21, No. 9, pp.1632,1643, Sept. 2013.

[8] L. Jing, P. Ndai, A. Goel, L. Haixin, K. Roy, "An alternate design paradigm for robust Spin-Torque Transfer Magnetic RAM (STT MRAM) from circuit/architecture perspective," *Design Automation Conference, 2009. ASP-DAC 2009. Asia and South Pacific* , Vol., No., pp.841,846, 19-22 Jan. 2009.

[9] D. Supriyo. *Quantum transport: atom to transistor*. Cambridge University Press,

2005.

[10] J. Knoch and J. Appenzeller, “Tunneling phenomena in carbon nanotube field-effect transistors,” *Phys. Stat. Sol. (A)*, vol. 205, no. 4, pp. 679–694, Apr. 2008.

[11] http://www.nobelprize.org/nobel_prizes/physics/laureates/2010/

[12] Son, Y. Woo, M. Cohen, and S. Louie. "Energy gaps in graphene nanoribbons." *Physical review letters* 97, no. 21 (2006).

[13] A. Raychowdhury, K. Roy, "A novel multiple-valued logic design using ballistic carbon nanotube FETs," *Multiple-Valued Logic, 2004. Proceedings. 34th International Symposium on* , Vol., No., pp.14,19, 19-22 May 2004.

[14] N. Mojumder, K. Roy, "Band-to-Band Tunneling Ballistic Nanowire FET: Circuit-Compatible Device Modeling and Design of Ultra-Low-Power Digital Circuits and Memories," *Electron Devices, IEEE Transactions on* , Vol. 56, No. 10, pp. 2193,2201, Oct. 2009.

[15] H. Raza, "Quantum Transport by Example, Second Tutorial, " http://user.engineering.uiowa.edu/~hraza/pdf/Tutorial_QT_Cornell_02.pdf

[16] S. Datta. "Nanoscale device modeling: the Green’s function method."*Superlattices and Microstructures*), pp. 253-278 (2000).

[17] http//quantumwise.com/

[18] K. Stokbro, D.E. Petersen, S. Smidstrup, A. Blom, M. Ipsen, and K. Kaasbjerg, *Phys. Rev. B*, **82**, 075420, 2010.

[19] M. Elstner, D. Porezag, G. Jungnickel, J. Elsner, M. Haug, T. Frauenheim, S. Su hai, and G. Seifert, *Phys. Rev. B*, **58**, 07260, 1998.

[20] Supriyo Datta (2008), "ECE 495N: Fundamentals of Nanoelectronics," https://nanohub.org/resources/5346.

[21] H. Raza, "Quantum Transport by Example, Third Tutorial, " http://user.engineering.uiowa.edu/~hraza/pdf/Tutorial_QT_Cornell_03.pdf

[22] Y. Chen, A. Rogachev, A. Sangai, G. Iannaccone, G. Fiori, D. Chen, "A SPICE-compatible model of Graphene Nano-Ribbon Field-Effect Transistors enabling circuit-level delay and power analysis under process variation," *Design,*

Automation & Test in Europe Conference & Exhibition (DATE), 2013 , pp. 1789-1794, 18-22 March 2013.

9. Appendix

9.1. Scilab® Code for Calculating Bandstructure of GNR

```
clear
pi =3.14
i=sqrt(-1)
a=3*1.44

Hnn=diag(zeros(1,500))
Hnm=diag(zeros(1,500))
ATK_Cor = read('atk_trans_1'+'.in',-1,3)        //Read ATK file to get co-ordinates of C-atoms
ATK_Cor(:,1)=ATK_Cor(:,1)*10                    //x-coordinates of atoms
ATK_Cor(:,2)=ATK_Cor(:,2)*21.074507697  //y-coordinates of atoms
ATK_Cor(:,3)=ATK_Cor(:,3)*106.5645          //z-coordinates of atoms
//Multiplication factor corresponds to unit vector

ATK_num=1:length(ATK_Cor(:,1))              //Total number of Carbon atoms
count=1

//Create Hnn ----------------------------------------------------------------------------------------------
//For each C atom calculate its distance from every other. If distance is equal to C-C bond, then
//they are nearest neighbor. Put to =3eV for every such pair, such that matrix row corresponds to
//the selected C atom and matrix column to the nearest neighbor atom.
//--------------------------------------------------------------------------------------------------------

for N_elem = 1:length(ATK_num)
   for N_elem_dist = 1:length(ATK_num)
      dist_m= sqrt(((ATK_Cor(N_elem,1)-
ATK_Cor(N_elem_dist,1))^2)+((ATK_Cor(N_elem,2)-
ATK_Cor(N_elem_dist,2))^2)+((ATK_Cor(N_elem,3)-ATK_Cor(N_elem_dist,3)))^2)

      count=count+1
      if dist_m <= 1.43   & dist_m >  0 then      //If distance corresponds to C-C bond

         Hnn(N_elem,N_elem_dist)= 3            //Put a to=3eV
      end
    end
end

//Create Hnm ----------------------------------------------------------------------------------------------
//Assume the unit cell is repeated to the left. Connect extreme left end of the current unit cell to
//corresponding extreme right end of assumed unit cell.
//--------------------------------------------------------------------------------------------------------

for N_elem = 1:length(ATK_num)
   if ATK_Cor(N_elem,3) == min(ATK_Cor(:,3)) then
      ATK_Cor(N_elem,3))
```

```
      for N_elem_pair = 1:length(ATK_num)
         if  ATK_Cor(N_elem_pair,3) == max(ATK_Cor(:,3)) &  ATK_Cor(N_elem,2)==
ATK_Cor(N_elem_pair,2) then
            Hnm(N_elem_pair,N_elem)=3
         end
      end
   end
end

kx = linspace(-pi/a,pi/a,2);                                    //Define range for kx
   for ik = 1:length(k);
      Hk = Hnn+Hnm*exp(i*k(ik)*a)+Hnm'*exp(-i*k(ik)*a);    // Equation 22
      [V Ek] = spec(Hk)
      w(:,ik) = gsort(diag(Ek),"r","i")
      xtitle('','kx','Energy(eV)')

   end
   plot(k,w)
```

9.2. Scilab ® Code for Modeling I_{ON} and I_{OFF}.

```
clear

pi=3.14
i=sqrt(-1)

KT = 4.11*1e-21                                  // Boltzman constant * 300K in Joules
q=1.6e-19                                        //Charge on electron
h=6.62e-34                                       //Planck's constant
h_bar=h/(2*pi)
mass=9.108 * 10^(-31)                            //Mass of electron

Eg=3.2*q                                         //Note in Joules.Number in eV. Bandgap
Edop = 25e-3*q
Vbi=0
Vds = 0.03
del_si_not_adjusted = [.6:.1:2]*q                //Tunneling window
eff_mass = 0.06*mass                             //Effective mass
lamda=2.7e-9                                     //Screening length

//Converting in row vectors ----------------------------------------------------------------------
del_si = del_si_not_adjusted - 0.62*q*ones(1:length(del_si_not_adjusted))
Eg_row= Eg*ones(1:length(del_si))
Edop_row = Edop*ones(1:length(del_si))
Vbi_row=Vbi*ones(1:length(del_si))
Vds_row = Vds*ones(1:length(del_si))
//-------------------------------------------------------------------------------------------------------------
```

```
Field = (Eg_row+del_si)/(q*lamda)

//Implementing equation 25----------------------------------------------------------------------------

T = exp(  (  -4 * sqrt(2*eff_mass) * ((Eg_row)^(3/2)) * lamda  ) ./ ( 3 * h_bar * (Eg_row + del_si)
)  )
//-------------------------------------------------------------------------------------------------------------

Ediff =Edop_row + Vbi_row + q*Vds_row

a= ( 1 + ( exp(- (Ediff/(KT)) ) ) )

b= ( 1 + ( exp( (-Edop_row + del_si) / (KT) ) ) )

c= ( 1 + ( exp( (-Ediff + del_si) / (KT) ) ) )

d= ( 1+ ( exp(-Edop_row/KT) ) )

I_on = (2*q*q/h_bar*2*pi) * T .* log(abs( (c .* d) ./ (a .* b) )) *1e-3 // Equation 26

plot(del_si_not_adjusted/q, log(abs(I_on)),'o')

//Modeling I_OFF----------------------------------------------------------------------------------
L=11.3e-9
Edop_off = 35e-3*q
Vbi_off=0
Vds_off = .1
del_si_not_adjusted_off = [0.0001:.05:.5]*q
eff_mass_off = 0.08*mass
lamda_off=2.7e-9

del_si_off = del_si_not_adjusted_off - 0*q*ones(1:length(del_si_not_adjusted_off))
Eb_row_off =( 1)*ones(1:length(del_si_off)) - 1*del_si_off/q//note volts sze Pg 392
Edop_row_off = Edop_off*ones(1:length(del_si_off))
Vbi_row_off=Vbi_off*ones(1:length(del_si_off))
Vds_row_off = Vds_off*ones(1:length(del_si_off))

T_off = (exp( (-2 * L * sqrt( 2*q*eff_mass_off*Eb_row_off ) ) /(h_bar) )) //Equation 27

I_off = 0.5*T_off*Vds_off                                    //Equation 28

plot(abs(del_si_off/q),log(I_off),'x')
```